Different Responses of Sea Surface Temperature in the South China Sea to Various El Niño Events during Boreal Autumn

WEI TAN

Institute of Physical Oceanography, Hohai University, Nanjing, China

XIN WANG

State Key Laboratory of Tropical Oceanography, South China Sea Institute of Oceanology, Chinese Academy of Sciences, Guangzhou, and Laboratory for Regional Oceanography and Numerical Modeling, Qingdao National Laboratory for Marine Science and Technology, Qingdao, China

WEIQIANG WANG

State Key Laboratory of Tropical Oceanography, South China Sea Institute of Oceanology, Chinese Academy of Sciences, Guangzhou, China

CHUNZAI WANG

NOAA/Atlantic Oceanographic and Meteorological Laboratory Miami, Florida

JUNCHENG ZUO

Institute of Physical Oceanography, Hohai University, Nanjing, China

(Manuscript received 8 May 2015, in final form 20 November 2015)

ABSTRACT

This study investigates variations of sea surface temperature (SST) anomalies in the South China Sea (SCS) during developing autumn of various El Niño events. The warm SST anomalies are observed in the SCS for canonical El Niño and El Niño Modoki I, whereas the cold SST anomalies are found for El Niño Modoki II. The ocean heat budget analyses show that the latent heat flux change induced by various types of El Niño events is a major contributor to the SCS SST variations. An anomalous anticyclone resides near the Philippine Sea for canonical El Niño and El Niño Modoki I, which induces the southerly wind anomalies over the SCS and thus weakens the climatological northeasterly in boreal autumn. The weakened surface wind speed reduces heat loss from the ocean, leading to a warmer state in the SCS. However, for El Niño Modoki II, the anomalous anticyclone shifts westward to the west of the SCS, and thus the northeasterly wind anomalies appear in the SCS. The northeasterly anomalies enhance the climatological northeasterly monsoon, increase the wind speed, and increase heat loss from the ocean, thus resulting in a cooling in the SCS. The anomalous anticyclone associated with El Niño events also increases shortwave radiation. The increases of the shortwave radiation can also contribute to the SCS warming for canonical El Niño and El Niño Modoki I in addition to the warm effect from the latent heat flux. Because the cooling effect from the latent heat flux is larger than that of the shortwave radiation for El Niño Modoki II, the SCS for El Niño Modoki II tends to be cool.

Publisher's Note: This article was revised on 12 February 2016 to include an additional email address in the corresponding author contact information.

Corresponding author address: Dr. Xin Wang, State Key Laboratory of Tropical Oceanography, South China Sea Institute of Oceanology, Chinese Academy of Sciences, 164 West Xingang Rd., Guangzhou 510301, China.
E-mail: wangxin@scsio.ac.cn; weiqiang.wang@scsio.ac.cn

DOI: 10.1175/JCLI-D-15-0338.1

1. Introduction

The South China Sea (SCS) is a semienclosed ocean basin in the western Pacific Ocean, which is an important passage linking the Pacific and Indian Oceans (Qu et al. 2000). The SCS is under the modulation of the East Asian monsoon. In winter, the SCS is dominated by the northeasterly monsoon, while the wind direction completely reverses to southwesterly in summer (Wyrtki 1961). In response to the northeasterly monsoon, the upper ocean circulation is generally cyclonic during winter. The summertime circulation is characterized by an anticyclonic gyre in the southern basin and a weak cyclonic gyre in the north (Shaw and Chao 1994; Shaw et al. 1999; Chu et al. 1999; Qu 2000; Yang et al. 2002). Correspondingly, the sea surface temperature (SST) in the SCS displays a strong seasonal cycle. The SST has a seasonal maximum in summer except for a "cool filament" due to the upwelling off the coast of South Vietnam (Xie et al. 2003) and then decreases in subsequent months and reaches its seasonal minimum in winter (Liu et al. 2002, 2004; Fang et al. 2006). Moreover, in response to the monsoon transition, a warm pool with the mixed layer temperature higher than 29°C is formed in the central SCS in spring and decays in June (Chu and Chang 1997; Wang and Wang 2006). The SCS SST variation can greatly influence extreme weather events and climate in the surrounding area on different time scales, such as the extreme daily temperature in summer (Gong et al. 2004), the summer monsoon onset (Ding et al. 2004; Kajikawa and Wang 2012; Liang et al. 2013; Xiang and Wang 2013), tropical cyclone activity (Wang et al. 2009; Ling et al. 2011), and rainfall by enhancing the convective instability (Chen et al. 2000; Ning and Qian 2009; Wu et al. 2010; Zhou et al. 2010).

It is well known that the SST variation in the SCS on interannual time scale is closely related to El Niño–Southern Oscillation (ENSO) (Tomita and Yasunari 1996; Ose et al. 1997; Qu et al. 2004; Wang et al. 2006). The SCS SST can be influenced by El Niño through the "atmospheric bridge" (Klein et al. 1999; Wang et al. 2000). The convective activity in the equatorial western Pacific shifts eastward during El Niño, which leads to an anomalous Walker circulation. These altered atmospheric circulations can directly modulate SST through surface heat fluxes (Trenberth et al. 1998; Klein et al. 1999; Wang et al. 2000; Alexander et al. 2002). On the other hand, the variations of the SCS SST anomalies are modulated by the ENSO-induced ocean dynamical processes (Qu et al. 2004). For the unprecedented warm event in the SCS during 1997–1999, Wang et al. (2002) found that the warm advection caused by the southerly wind anomalies mainly contributes to its development, and the maintenance is primarily due to the deeper thermocline. The El Niño signal can be conveyed into the SCS through Luzon Strait (Qu et al. 2004; Tian et al. 2006) and Mindoro Strait (Liu et al. 2011). Through the abovementioned ways, the SCS SST is warmer (cooler) during El Niño (La Niña) events and reaches a maximum (minimum) lagging the ENSO peak phase by 1–2 seasons (Klein et al. 1999). Moreover, Wang et al. (2006) discovered the feature of a double-peak evolution of the SCS SST anomalies associated with El Niño events and investigated the mechanisms. The first peak occurs in February in the decaying year of El Niño, which mainly results from shortwave radiation and latent heat flux anomalies. The second peak is around subsequent August, which is attributed to the mean meridional geostrophic heat advection. A persistence barrier of the SCS SST is found in boreal fall around October and November, which is vigorous in developing autumn of strong El Niño events (Chen et al. 2007). The occurrence of the persistence barrier as well as the rapid warming of the SCS during fall of strong El Niño are mainly attributed to the evolution of the low-level anomalous anticyclone, which in turn increases the solar heating in October and decreases the evaporative cooling in November and December (Chen et al. 2007). Comparing the relative contributions of El Niño and the East Asian winter monsoon (EAWM) to the SCS SST anomalies in the subsequent years, Wu et al. (2014) revealed that the SST anomalies during January–March are mostly related to the EAWM variability, whereas ENSO plays a dominant role in decaying summer.

Recently, a new type of El Niño called El Niño Modoki (Ashok et al. 2007) has been emphasized, with its maximum SST anomalies located in the tropical central Pacific instead of in the tropical eastern Pacific as for canonical El Niño. El Niño Modoki is also termed date line El Niño (Larkin and Harrison 2005), central Pacific El Niño (Yu and Kao 2007), and warm pool El Niño (Kug et al. 2009). In this paper, the name El Niño Modoki is used. El Niño Modoki occurs more frequently since the 1990s (Ashok et al. 2007; Kao and Yu 2009; Yeh et al. 2009), and the intensity is increasing in the past three decades (Lee and McPhaden 2010). Because of different warming locations and intensities between canonical El Niño and El Niño Modoki, significant differences exist in the anomalous atmospheric circulations and their influences on the tropical and extratropical climate (Weng et al. 2007; Kao and Yu 2009; Kug et al. 2009; Kim et al. 2012). Some literature has studied and compared different responses of the SCS climate to the two types of El Niño events (Hong et al. 2011; Wang et al. 2014; Liu et al. 2014). Although the SCS SST anomalies exhibit a warm double-peak evolution, the areas and intensities of warm SST anomalies are relatively weaker during El Niño Modoki than those during canonical El Niño (Liu et al. 2014).

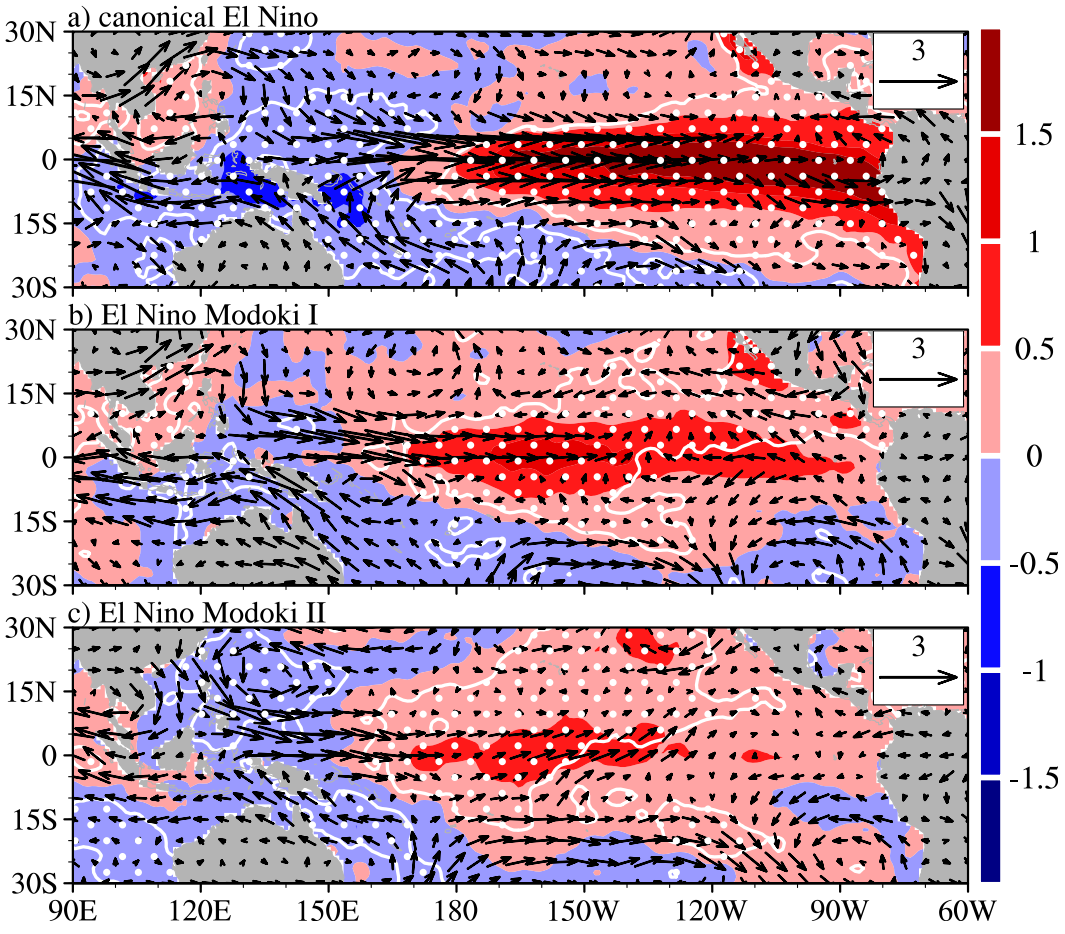

FIG. 1. Composited SST anomalies (shading; °C) and 850-hPa wind anomalies (vector; m s^{-1}) during boreal autumn for (a) canonical El Niño, (b) El Niño Modoki I, and (c) El Niño Modoki II. The white contours filled with dots indicate the composite exceeding the 90% significance level based on a Student's *t* test. The HadISST dataset and NCEP–NCAR reanalysis are used for SST and 850-hPa wind speed, respectively.

Based on opposite impacts on rainfall in southern China in boreal fall, El Niño Modoki events can be further separated into two groups: El Niño Modoki I and II (Wang and Wang 2013). As demonstrated in Wang and Wang (2013), using ±0.5 standard deviation of the autumn-averaged rainfall anomalies in southern China as a threshold, El Niño Modoki I (II) can be identified when the rainfall anomalies are larger (lower) than +0.5 (−0.5) standard deviations. Moreover, they exhibit different spatial patterns of SST anomalies (Wang and Wang 2013). For canonical El Niño, warm SST anomalies originate from the equatorial eastern Pacific along the South American coast in boreal spring and then strengthen and develop westward (Rasmusson and Carpenter 1982) and finally reach a mature phase with peak values in the equatorial eastern Pacific in boreal winter. Although the warm SST anomalies reach peak in the equatorial central Pacific in winter for both El Niño Modoki I and II, the origins and evolutions are different. For El Niño Modoki I, the warm SST anomalies are first found in the equatorial central Pacific, and then intensify and eventually reach a peak locally, whereas for El Niño Modoki II, the warm SST anomalies originate in the subtropical northeastern Pacific and then develop southwestward to the equatorial central Pacific. Wang and Wang (2013) showed that the significantly different spatial patterns of SST anomalies appear in autumn. Figure 1 shows the composited SST anomalies and low-level wind anomalies during boreal autumn for three types of El Niño events. The differences of SST anomalies lead to different atmospheric responses (Fig. 1). Because of the Rossby wave response, for canonical El Niño there is an anomalous anticyclone over the Philippine Sea during autumn (Fig. 1a) (Weisberg and Wang 1997; Wang et al. 1999, 2000). A similar anticyclone also exists for El Niño Modoki I, but with a weaker magnitude (Fig. 1b). In contrast, an anomalous cyclone resides near the Philippine Sea for El Niño Modoki II

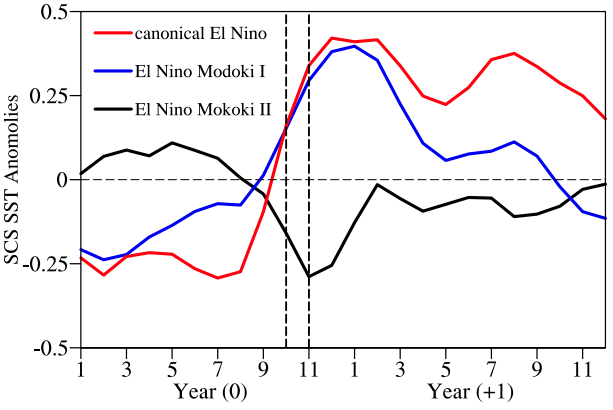

FIG. 2. The evolution of the composite SST anomalies (°C) averaged in the SCS during canonical El Niño (red), El Niño Modoki I (blue), and El Niño Modoki II (black). The two dashed lines indicate October and November in year(0); year(0) means the developing year of El Niño, and year(+1) is the subsequent year.

(Fig. 1c). Furthermore, these atmospheric responses could have different impacts on the Indian Ocean dipole (IOD) (Wang and Wang 2014).

The response of the SCS SST anomalies to canonical El Niño is well studied, but quite little is known about the impacts of El Niño Modoki events on the SCS SST. The purpose of this study is to investigate the variations of the SCS SST anomalies associated with canonical El Niño and El Niño Modoki I and II, and the corresponding physical mechanisms. The results are expected to improve the understanding of the interannual variation of the SCS SST. The study focuses on boreal autumn [October–November (ON)] because the warm SST anomalies of three types of El Niño events in the tropical Pacific are significantly different during this season (Wang and Wang 2013).

The paper is organized as follows. A brief description of the datasets, methods, and numerical model used in this study is given in section 2. Section 3 presents the variations of the SCS SST anomalies associated with various El Niño events. Section 4 performs a heat budget analysis to investigate atmospheric and oceanic processes generating the SCS SST anomalies during various types of El Niño events, followed by the explanations of how various types of El Niño events influence these processes in section 5. Several numerical simulations are performed to corroborate our observed results in section 6. Finally, a summary along with discussion is presented in section 7.

2. Datasets, methods, and numerical model

a. Datasets

In this study, the monthly ocean temperature, wind stress and sea surface height (SSH) from the Simple Ocean Data Assimilation (SODA), version 2.1.6, from 1958 to 2008 (Carton and Giese 2008) and surface heat fluxes obtained from the Japanese 55-Year Reanalysis Project (JRA-55) with a resolution of 0.5625° × 0.5625° (TL319L60, horizontal spectral resolution with 60 vertical levels) from 1958 to 2013 (Ebita et al. 2011) are used for the heat budget analysis. The SODA dataset has a resolution of 0.5° × 0.5° and 40 vertical levels ranging from 5 to 5375 m. For the overlapping time period, the ocean heat budget is performed using all these datasets from 1958 to 2008. The monthly 10-m wind speed and air–sea difference in saturated specific humidity provided by International Comprehensive Ocean–Atmosphere Dataset (ICOADS) with a resolution of 1° × 1° from 1960 to 2014 (Woodruff et al. 2011) are used to analyze the variations of the latent heat flux. The total cloud cover from the National Centers for Environmental Prediction (NCEP)–National Center for Atmospheric Research (NCAR) reanalysis (1948–present) is adopted (Kalnay et al. 1996) to analyze the shortwave radiation flux variations. In addition, the monthly Hadley Centre Sea Ice and Sea Surface Temperature (HadISST) dataset with a resolution of 1° × 1° from 1870 to 2015 (Rayner et al. 2003) is used to validate variations of the SCS SST during various types of El Niño events.

For all of these datasets, anomalies are computed as departures from the 1971–2000 climatology, and a linear trend is removed before the analyses. The three types of El Niño events are identified according to Wang and Wang (2013). During the study period (1958–2008), there are five canonical El Niño events (1965/66, 1972/73, 1976/77, 1982/83, and 1997/98), four El Niño Modoki I events (1963/64, 1987/88, 1990/91, and 2002/03), and five El Niño Modoki II events (1968/69, 1979/80, 1991/92, 1992/93, and 2004/05).

b. Methods

In this study, the composite analysis is applied with a Student's t test. To identify the relative contributions of physical processes inducing SST anomaly variations in autumn during three types of El Niño events, an upper ocean heat budget analysis is performed. After linearizing the SST equation (Qiu 2000) and ignoring the second-order infinitesimal terms, the heat balance equation of SST anomalies can be described as

$$\frac{\partial T'}{\partial t} = \frac{Q'_{\mathrm{NET}}}{\rho C_p \overline{h}} - (\overline{\mathbf{u}}_E \cdot \nabla T' + \mathbf{u}'_E \cdot \nabla \overline{T}) - (\overline{\mathbf{u}}_G \cdot \nabla T' + \mathbf{u}'_G \cdot \nabla \overline{T}) - \left[\overline{w}_E \frac{(T - T_d)'}{\overline{h}} + w'_E \frac{\overline{T - T_d}}{\overline{h}} \right] + \mathrm{RES}. \quad (1)$$

This equation is consistent with Liu et al. (2014). The overbar denotes the climatological mean, and the prime

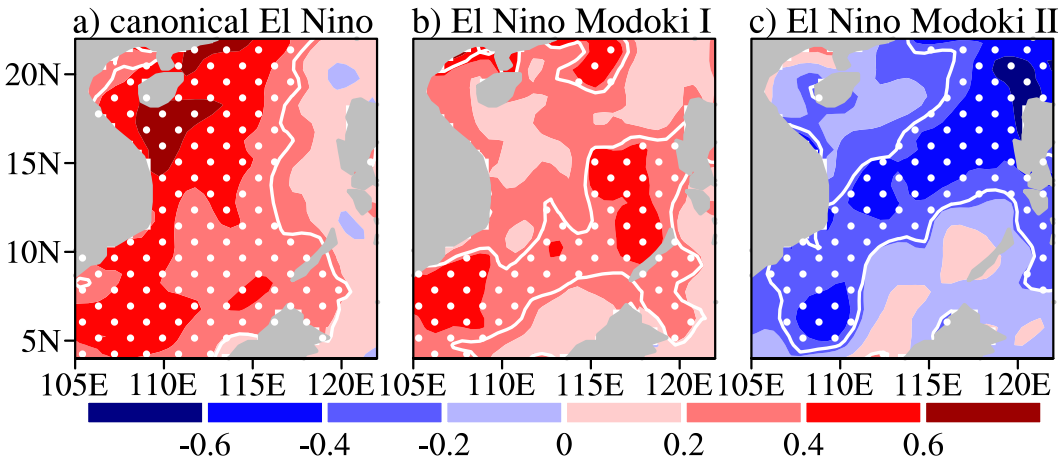

FIG. 3. Composites of SST anomalies (°C) during developing autumn (ON) of (a) canonical El Niño, (b) El Niño Modoki I, and (c) El Niño Modoki II. The white contours and the area filled with white dots indicate the composite exceeding the 90% significant level, based on a Student's t test. The SST from SODA (version 2.1.6) was used (Carton and Giese 2008).

corresponds to the anomaly; T is the mixed layer temperature, and it is a good proxy for SST (Qiu 2000); Q_{NET} is the net surface heat flux, ρ is the seawater density ($1025\,\mathrm{kg\,m^{-3}}$), C_p is the specific heat capacity ($3890\,\mathrm{J\,kg^{-1}\,K^{-1}}$), and h is the mixed layer depth (MLD). In this study, the MLD is defined as the depth at which the temperature is 0.5°C lower than the surface temperature (Monterey and Levitus 1997). The horizontal circulation in the surface mixed layer can be divided into Ekman current $\mathbf{u}_E$ and geostrophic current $\mathbf{u}_G$; $\mathbf{u}_E$ is driven by the surface wind stress $\boldsymbol{\tau}\times\mathbf{k}/\rho f\overline{h}$, and $\mathbf{u}_G$ is governed by the horizontal pressure gradient $-g\nabla\eta\times\mathbf{k}/f$, where g is the gravitational acceleration, f is the Coriolis parameter, and η means SSH. Also, w_E is the entrainment velocity. Because of the shallow MLD in the SCS, the entrainment velocity is dominated by Ekman pumping $\nabla\times\tau/\rho f$ (Qu 2001; Wang and Wang 2006). Finally, T_d is the temperature at a depth of 5 m below the bottom of the mixed layer.

On the right-hand side of Eq. (1), the first term represents the net heat flux anomaly forcing. Ekman heat advection is divided into mean Ekman heat advection (the second term) and anomalous Ekman heat advection (the third term). Geostrophic heat advection is the sum of the fourth and fifth terms, which represent mean geostrophic heat advection and anomalous geostrophic heat advection, respectively. Entrainment heat flux includes the mean entrainment heat advection (the sixth term) and anomalous entrainment heat advection (the seventh term). The last term denotes the residual term

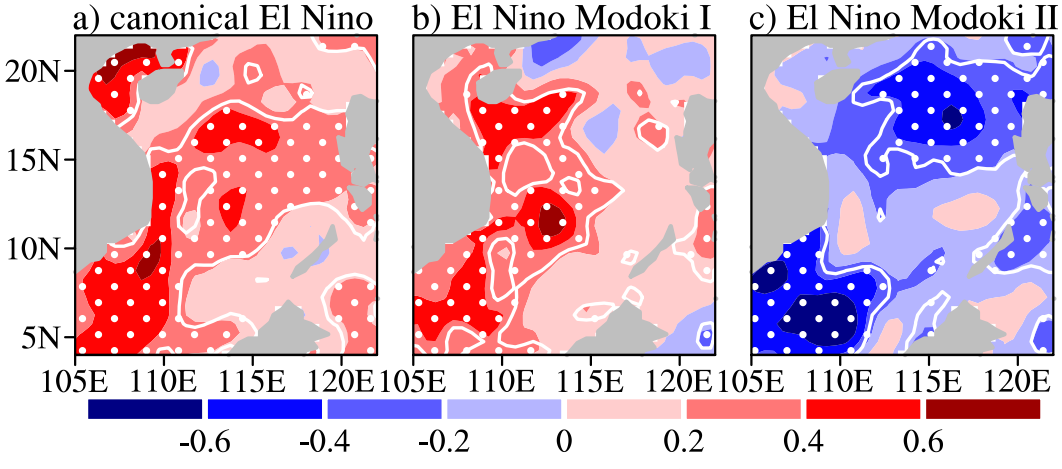

FIG. 4. As in Fig. 3, but for SST anomaly tendencies ($\partial T'/\partial t$; °C month^{-1}) for three types of El Niño events. The tendency is calculated by the difference between the SST anomalies in November and October.

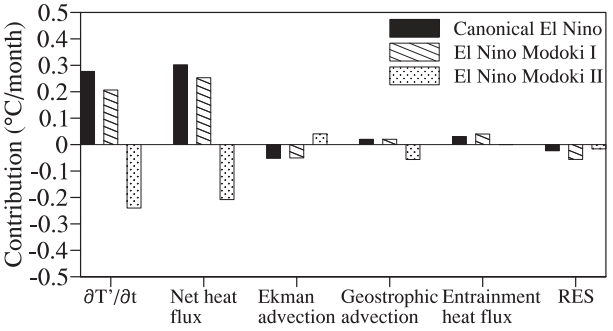

FIG. 5. Contributions of atmospheric and oceanic processes to SST tendency averaged in the SCS (°C month^{-1}). Positive heat flux indicates that the ocean obtains heat from the atmosphere. All these terms are averaged between October and November except for $\partial T'/\partial t$, which is defined as the difference between October and November.

(RES), which includes nonlinear heat advection and diffusion, etc.

c. *Numerical model*

The Community Atmosphere Model, version 4 (CAM4; Neale et al. 2013), is used to examine the atmospheric response to the tropical heating. CAM4 is the sixth generation of the atmospheric general circulation model (AGCM) developed at NCAR, and it is the atmosphere component of the Community Climate System Model (Gent et al. 2011). Compared with CAM3, CAM4 has significant improvements to the dynamical core, deep convective parameterization, and cloud fraction calculation (Neale et al. 2013). In this study, the default finite volume dynamical core is used and a relatively lower spatial resolution is adopted (1.9° × 2.5°) with 26 vertical levels for computational resource limitation.

3. SCS SST anomaly variations in various types of El Niño events

The temporal evolution of the SCS SST anomalies during three types of El Niño events is displayed in Fig. 2. The changes of SCS SST anomalies associated with canonical El Niño are consistent with previous studies. A double-peak evolution can be seen during canonical El Niño, which is similar to the results of Wang et al. (2006). A salient feature in Fig. 2 is that the SCS SST anomalies begin to be warming (cooling) from October for canonical El Niño and El Niño Modoki I (El Niño Modoki II), and these warming (cooling) SST anomalies could be persistent to next autumn. Figure 2 shows that the rapid increase (decrease) of SST anomalies for canonical El Niño and El Niño Modoki I (El Niño Modoki II) appears in autumn. Chen et al. (2007) suggested that the rapid warming of the SCS during fall of strong El Niño is mainly attributed to the evolution of the low-level anomalous anticyclone, which in turn increases the solar heating in October and decreases the evaporative cooling in November and December. In addition, Chen et al. (2007) found a persistence barrier of the SCS SST in boreal fall around October and November, which is vigorous in developing autumn of strong El Niño events. Therefore, the study analyzes the changes of the SCS SST associated with various types of El Niño events in autumn (October–November).

The composites of the SST anomalies in the SCS during developing October–November of various El Niño events are shown in Fig. 3. For canonical El Niño, a basin-scale warming is seen in the SCS, the warm center is located in the western SCS, and the maximum of SST anomalies reaches up to 0.6°C (Fig. 3a). Similar to canonical El Niño, the warm SST anomalies are also

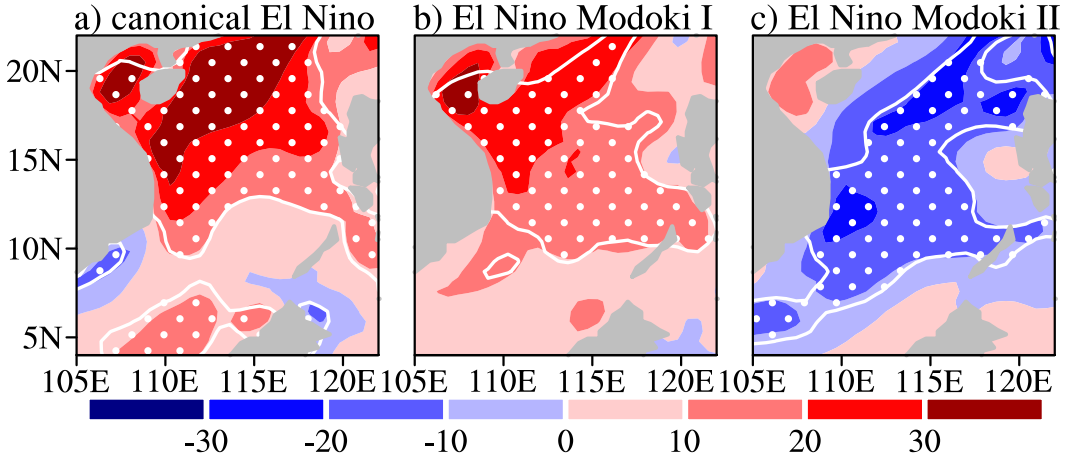

FIG. 6. As in Fig. 4, but for net heat flux anomalies (W m^{-2}) averaged between October and November for three types of El Niño events.

observed across the SCS for El Niño Modoki I. The significantly warm SST anomalies (up to 0.6°C) are in the southern and central SCS (Fig. 3b). However, for El Niño Modoki II, the significantly cold SST anomalies appear in the northeastern–southwestern SCS, with the cold centers (up to −0.6°C) being located near Luzon Strait (Fig. 3c). It is noted that the composites of SST anomalies calculated from HadISST show similar results (not shown).

4. Heat budget analysis of the SCS SST anomalies

The tendencies of the SCS SST anomalies during boreal autumn associated with various El Niño events are shown in Fig. 4. Here, the SCS SST anomaly tendency in autumn means the SST anomaly differences between November and October. For canonical El Niño, the basin-scale warming tendency in the SCS is observed, and the significantly warming tendencies are in the northwestern, central, and southwestern SCS (Fig. 4a). Although the warming tendency in the whole SCS basin for El Niño Modoki I is similar to that for canonical El Niño, differences are seen. The significantly warming tendency for El Niño Modoki I appears in the western SCS, confined to the west of 115°E (Fig. 4b), which is different from canonical El Niño. Different from the warming tendencies for canonical El Niño and El Niño Modoki I, the basin-scale cooling tendency is seen in the SCS for El Niño Modoki II. The significantly cooling tendency is located in the northern and southwestern SCS (Fig. 4c).

To compare the contributions of atmospheric and oceanic processes to the SCS SST changes for various El Niño events, a mixed layer heat budget analysis is performed using monthly variables (Fig. 5). In this study, the corresponding dynamic and thermodynamic terms on the right-hand side of Eq. (1) are all averaged between October and November. In addition, downward for heat flux is set the positive direction. That is to say, positive heat flux indicates that the ocean obtains heat from the atmosphere. From the heat budget averaged over the SCS, the SCS warming tendency for canonical El Niño is dominantly attributed to the net surface heat flux (near 0.3°C month^{-1}), consistent with the results of Wang et al. (2006). Like the situation of canonical El Niño, the net surface heat flux plays the most important warming and cooling roles for El Niño Modoki I and II, respectively. It should be noted that similar conclusions are also derived using other surface heat flux products such as NCEP (not shown). Compared with the contributions of net surface heat flux, the contributions of Ekman advection, geostrophic advection, and vertical entrainment are small for three types of El Niño events

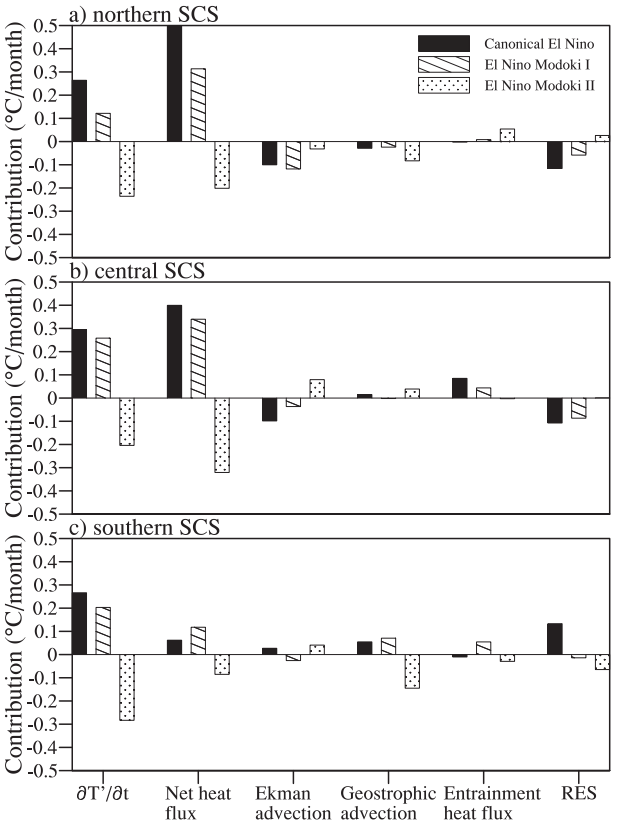

FIG. 7. Contributions of atmospheric and oceanic processes to SST tendency (°C month^{-1}) averaged in the (a) northern, (b) central, and (c) southern SCS. Positive heat flux indicates that the ocean obtains heat from the atmosphere. All these terms are averaged between October and November except for $\partial T'/\partial t$, which is defined as the difference between October and November.

(less than 0.05°C month^{-1}). Although the contributions of Ekman current and geostrophic current to SST variations are greatly less than these of the net heat flux, some interesting results are seen in Fig. 5. The contribution of Ekman advection is opposite to that of geostrophic advection for three types of El Niño events, indicating that the total contributions of ocean horizontal circulations are close to zero. In addition, the SST variations induced by Ekman advection and geostrophic advection exhibit obvious differences for three types of El Niño events. For canonical El Niño and El Niño Modoki I, the Ekman (geostrophic) current tends to cool (warm) the SCS, while for El Niño Modoki II the contribution of Ekman (geostrophic) current is opposite to that for canonical El Niño and El Niño Modoki I. This suggests that the responses of oceanic horizontal circulations in the SCS to three types of El Niño events are different. This issue will be addressed in other study.

Based on the heat budget analysis, we found that the SCS-averaged net heat flux is responsible for the SCS

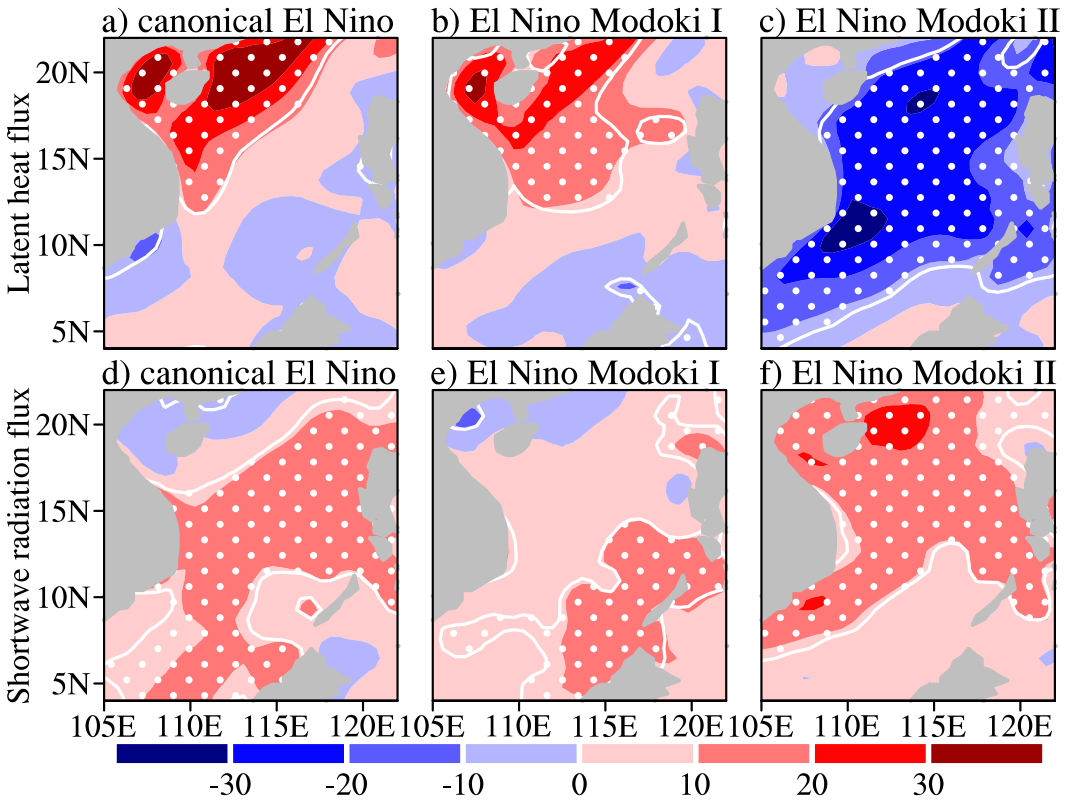

FIG. 8. Composites of the (top) latent heat flux anomalies ($W\,m^{-2}$) and (bottom) shortwave radiation flux anomalies ($W\,m^{-2}$) averaged between October and November for (a),(d) canonical El Niño, (b),(e) El Niño Modoki I, and (c),(f) El Niño Modoki II. The white contours and the area filled with white dots indicate the composite exceeding the 90% significance level, based on a Student's *t* test.

SST variations for various types of El Niño events. The spatial patterns of the net heat flux over the SCS in autumn for three types of El Niño events are shown in Fig. 6. For canonical El Niño, the positive net heat flux anomalies are observed in most of the SCS, which leads to the warming SCS. The significantly warm centers are located in the northern SCS, and the maximum is more than $30\,W\,m^{-2}$ (Fig. 6a). Compared with Fig. 6a, the pattern of the net heat flux anomalies associated with El Niño Modoki I is similar to that of canonical El Niño, while the intensity is weaker (Fig. 6b). The weaker amplitude of heat flux anomalies for El Niño Modoki I is suggested to be attributed to the weaker warm SST anomalies in the tropical Pacific (Wang and Wang 2013). In contrast, the significantly negative anomalies are in most of the SCS for El Niño Modoki II (Fig. 6c), indicating that heat is released from the ocean to atmosphere, and thus the SST tends to be cooling.

Although the net heat flux averaged in the whole basin could account for the SST tendencies well, there still exist some differences in the spatial patterns (Figs. 4 and 6). For example, the net heat flux anomalies of both canonical El Niño and El Niño Modoki I mainly exhibit major positive anomaly centers in the northern and central SCS (Figs. 6a,b), while the warming tendencies appear in the southern SCS (Figs. 4a,b). For El Niño Modoki II, although the significantly negative net heat flux anomalies are in most of the SCS basin (Fig. 6c), the cooling tendency is relatively weak between 10° and 15°N (Fig. 4c). To evaluate the contributions in detail, we separate the SCS into three parts: the southern SCS (4°–10°N), the central SCS (10°–18°N), and the northern SCS (18°–22°N). The contributions averaged in these three parts are illustrated in Fig. 7. Similar to Fig. 5, both the northern SCS (Fig. 7a) and central SCS (Fig. 7b) are governed by the net heat flux for three types of El Niño events. The geostrophic heat advection plays a secondary role in the northern SCS during El Niño Modoki II, and the entrainment heat flux is secondary in the central SCS during canonical El Niño and El Niño Modoki I. It is noted that the Ekman heat advection could result in warm SST anomalies, and thus offset about one-third of the cooling effect induced by net heat flux in the central SCS for El Niño Modoki II (Fig. 7b). However, in the

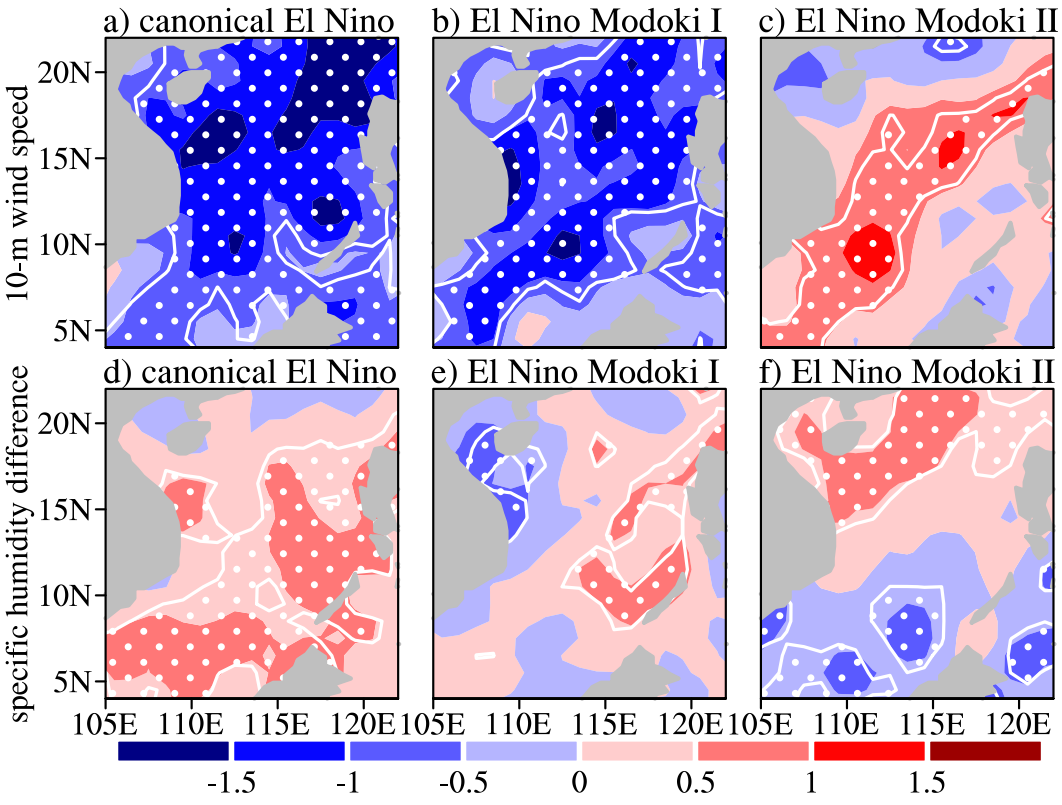

FIG. 9. Composites of (top) 10-m wind speed anomalies ($m\,s^{-1}$) and (bottom) anomalous air–sea differences in specific humidity ($g\,kg^{-1}$) averaged between October and November for (a),(d) canonical El Niño, (b),(e) El Niño Modoki I, and (c),(f) El Niño Modoki II. The white contours and the area filled with white dots indicate the composite exceeding the 90% significance level, based on a Student's *t* test.

southern SCS, the contributions of the geostrophic advection become more important. The contributions of the geostrophic advection terms are comparable to these of the net heat flux terms for three types of El Niño events, which may be related to the strong geostrophic currents over there (Xie et al. 2003). In particular, the geostrophic advection even plays a dominant role during El Niño Modoki II (Fig. 7c). The significantly negative geostrophic advection occurs around the Sunda Shelf (not shown). Because of space limitation, we mainly focus on the central and northern SCS, where the net heat flux is the major contributor. The southern SCS will be discussed in future study.

The net surface heat flux includes shortwave radiation, longwave radiation, latent heat flux, and sensible heat flux. Because of the small magnitudes of longwave radiation and sensible heat flux in the SCS (Gupta et al. 1999; Chou et al. 2000; Zhang et al. 2012), latent heat flux and shortwave radiation flux anomalies are analyzed in this paper. For three types of El Niño events, amplitudes of latent heat flux anomalies (Figs. 8a–c) are all larger than these of the shortwave radiation flux anomalies (Figs. 8d–f), especially for El Niño Modoki II. The spatial patterns of the latent heat flux anomalies for three types of El Niño events are similar to these of the net heat flux anomalies. The positive anomalies of latent heat flux are significant in the northern SCS for canonical El Niño and El Niño Modoki I, and the significantly negative anomalies appear in the whole basin for El Niño Modoki II. Therefore, the SCS SST tendencies for three types of El Niño events are mainly controlled by the variations of latent heat flux anomalies. Shortwave radiation flux plays the secondary role in the SCS SST changes. Next, the mechanisms of how three types of El Niño events result in the changes of the latent heat flux in the SCS are analyzed.

5. Mechanisms of El Niño–induced heat flux changes in the SCS

Since the latent heat flux is a major contributor to the SCS SST changes, this section focuses on the mechanisms of how various El Niño events affect the latent heat flux over the SCS. In addition, the anomalous shortwave radiation flux in the SCS associated with various types of El Niño events is also discussed.

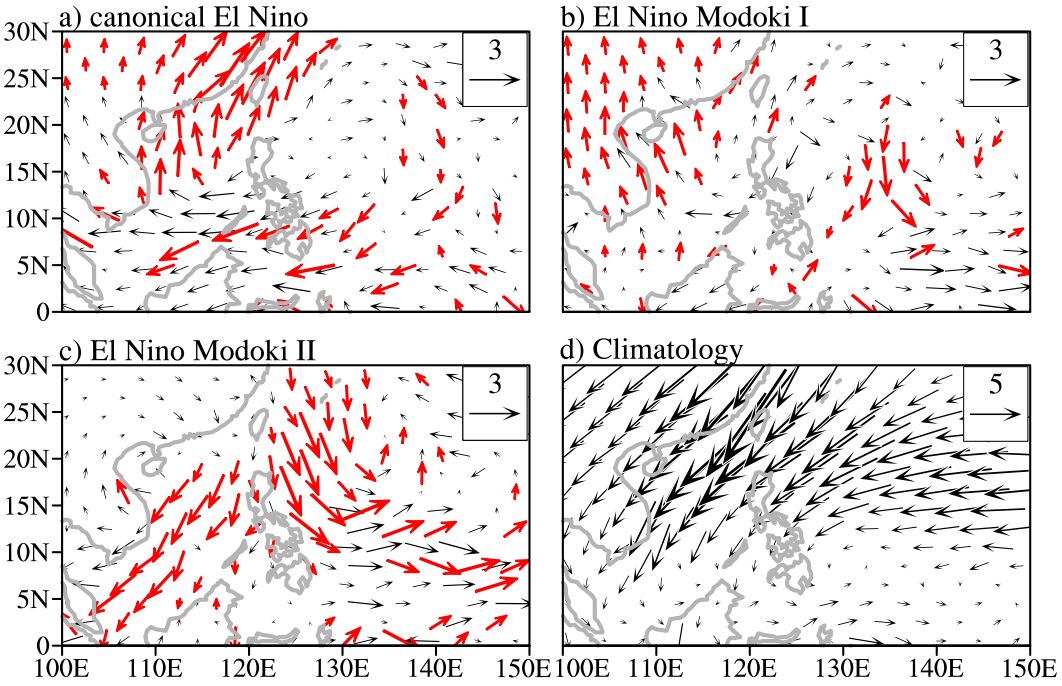

FIG. 10. Composites of 10-m wind anomalies ($m\,s^{-1}$) averaged between October and November for (a) canonical El Niño, (b) El Niño Modoki I, (c) El Niño Modoki II, and (d) 10-m wind climatology during October and November. The red arrows indicate meridional wind speed exceeding the 90% significance level.

The changes of the latent heat flux are greatly influenced by large-scale atmospheric circulations. The latent heat flux is associated with 10-m wind speed and air–sea specific humidity difference (Chou et al. 2000; Wang et al. 2006). The heat from the ocean to the atmosphere is easily released with large wind speed and high air–sea specific humidity difference for cooling the sea surface. The anomalous 10-m wind speeds and air–sea specific humidity differences associated with various El Niño events are shown in Fig. 9. It is seen that the 10-m wind speed anomalies are significantly different over the SCS. For canonical El Niño and El Niño Modoki I, the wind speeds are significantly reduced (Figs. 9a and 9b). However, for El Niño Modoki II, the significantly enhancing wind speeds appear in the northeastern–southwestern SCS (Fig. 9c), which favors surface cooling (Fig. 4c). Specific humidity differences between the air and ocean for various El Niño events show few differences. The positive specific humidity differences between the air and ocean cover nearly the whole SCS, except for weakly negative values in the western SCS for El Niño Modoki I and the southern SCS for El Niño Modoki II (Figs. 9d–f). Therefore, the differences of the latent heat flux are mainly attributed to the surface wind speed over the SCS for three types of El Niño events.

To explain the weak or strong wind speeds over the SCS for three types of El Niño events in Fig. 9, we calculate the composites of the low-level atmospheric circulations over the SCS (Fig. 10). As discussed in Fig. 1, for canonical El Niño and El Niño Modoki I, an anomalous anticyclone appears near the Philippine Sea (Figs. 10a,b) due to the Rossby wave response to ENSO (Weisberg and Wang 1997; Wang et al. 1999; Wang et al. 2000; Wang et al. 2012, 2014). The SCS is located in the west of the anomalous anticyclone center and thus is significantly influenced by southerly wind anomalies. It is noted that the intensity of the anticyclonic circulation for El Niño Modoki I is weaker than that for canonical El Niño. Climatologically, the northeasterly wind prevails over the SCS in boreal autumn (Fig. 10d). The southerly anomalies associated with canonical El Niño and El Niño Modoki I weaken the climatological northeasterly wind, and thus the wind speed is reduced (Figs. 9a,b), leading to the positive latent heat flux anomalies (Figs. 8a,b). In contrast, for El Niño Modoki II, a significantly anomalous cyclone resides east of the Philippines, and the anomalous anticyclone shifts westward to southern East Asia (Fig. 10c), which is due to the pattern of warm SST anomalies extending from the northeastern Pacific to the equatorial central Pacific and farther westward in the equatorial central Pacific compared with El Niño Modoki I (Wang and Wang 2013). The SCS is in the east of the anomalous anticyclone center and thus is dominated by the northeasterly

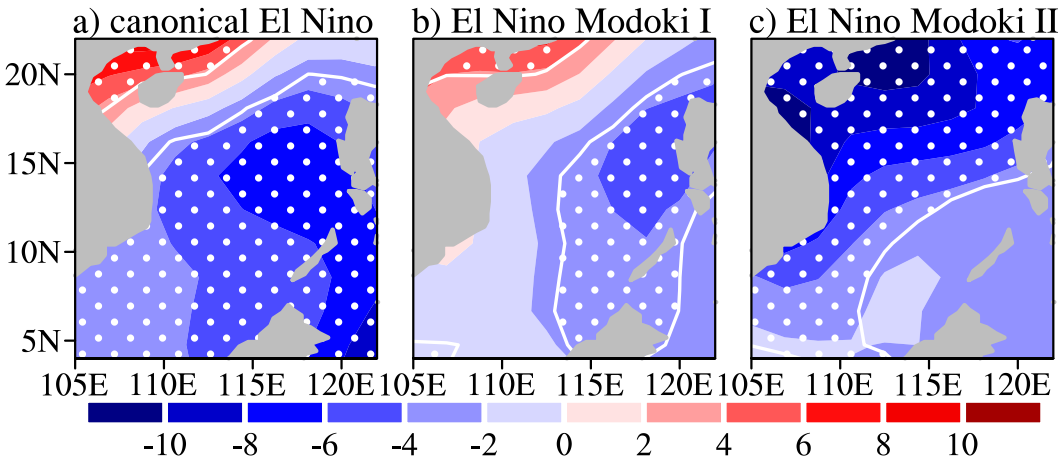

FIG. 11. Composites of total cloud cover anomalies (%) averaged between October and November for (a) canonical El Niño, (b) El Niño Modoki I, and (c) El Niño Modoki II. The white contours and the area filled with white dots indicate the composite exceeding the 90% significance level, based on a Student's *t* test.

wind anomalies. Such anomalous northeasterly winds combined with the climatological northeasterly monsoon increase wind speed (Fig. 9c) and thus drive more latent heat released from the ocean (Fig. 8c).

In addition to the impacts of the low-level wind speed, the anomalous anticyclone over the SCS for three types of El Niño events can also influence the shortwave radiation variations. The anomalous anticyclone may suppress convective activity and significantly reduce the cloud cover (Fig. 11), which increases shortwave radiation (Figs. 8d–f). For canonical El Niño and El Niño Modoki I, the decreases of low-level wind speed combined with the increases of shortwave radiation contribute to the warm tendency of the SCS SST anomalies. Although the shortwave radiation is also increased due to the decreased cloud cover for El Niño Modoki II, its magnitude (Fig. 8f) is smaller than that of the latent heat flux induced by increased wind speed (Fig. 8c). Therefore, negative net heat flux anomalies appear in the SCS for El Niño Modoki II (Fig. 6c).

6. Model experiments of El Niño–induced atmospheric circulation

To further identify different atmospheric responses to three types of El Niño events, we perform four CAM4 model experiments. The first experiment is forced by the climatological mean SST with a 32-yr integration, referred to as control run, and the model results of the last 30 years are used to calculate the climatology. The other three experiments are sensitivity experiments. It should be noted that the warm SST anomalies in the tropical Pacific are significantly different during boreal autumn (Wang and Wang 2013), and the distinct differences of the SCS SST anomalies also appear in developing autumn (Fig. 2). Therefore, these three sensitivity experiments are driven by the climatological SST with SST anomalies in different regions in boreal fall (September–November). According to the significant SST anomalies for the three types of El Niño events in Fig. 1, the idealized SST anomalies of 2°C in the tropical eastern Pacific (10°S–10°N, 120°–80°W) and 1.5°C in the central Pacific (10°S–10°N, 170°–130°W) are used to force the model for canonical El Niño and El Niño Modoki I, respectively (Fig. 12). For El Niño Modoki II, the SST anomalies of 1.5°C in the parallelogram-like region from the subtropical northeastern Pacific to the tropical central Pacific are prescribed. All of these three sensitivity experiments are integrated for 16 years, and the last 10 years are analyzed.

The differences of the sea level pressure (SLP) and low-level (850 hPa) wind anomalies averaged in boreal autumn (October and November) between sensitivity and control experiments (Fig. 13) are consistent with the

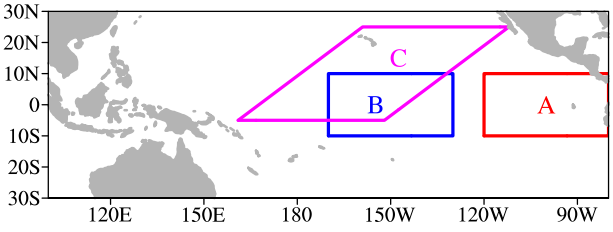

FIG. 12. The idealized SST anomalies used to force the three sensitivity experiments. The warming area is within 10°S–10°N, 120°–80°W for canonical El Niño (red box denoted with A) and within 10°S–10°N, 170°–130°W for El Niño Modoki I (blue box denoted with B); the parallelogram-like region is for El Niño Modoki II (magenta parallelogram denoted with C).

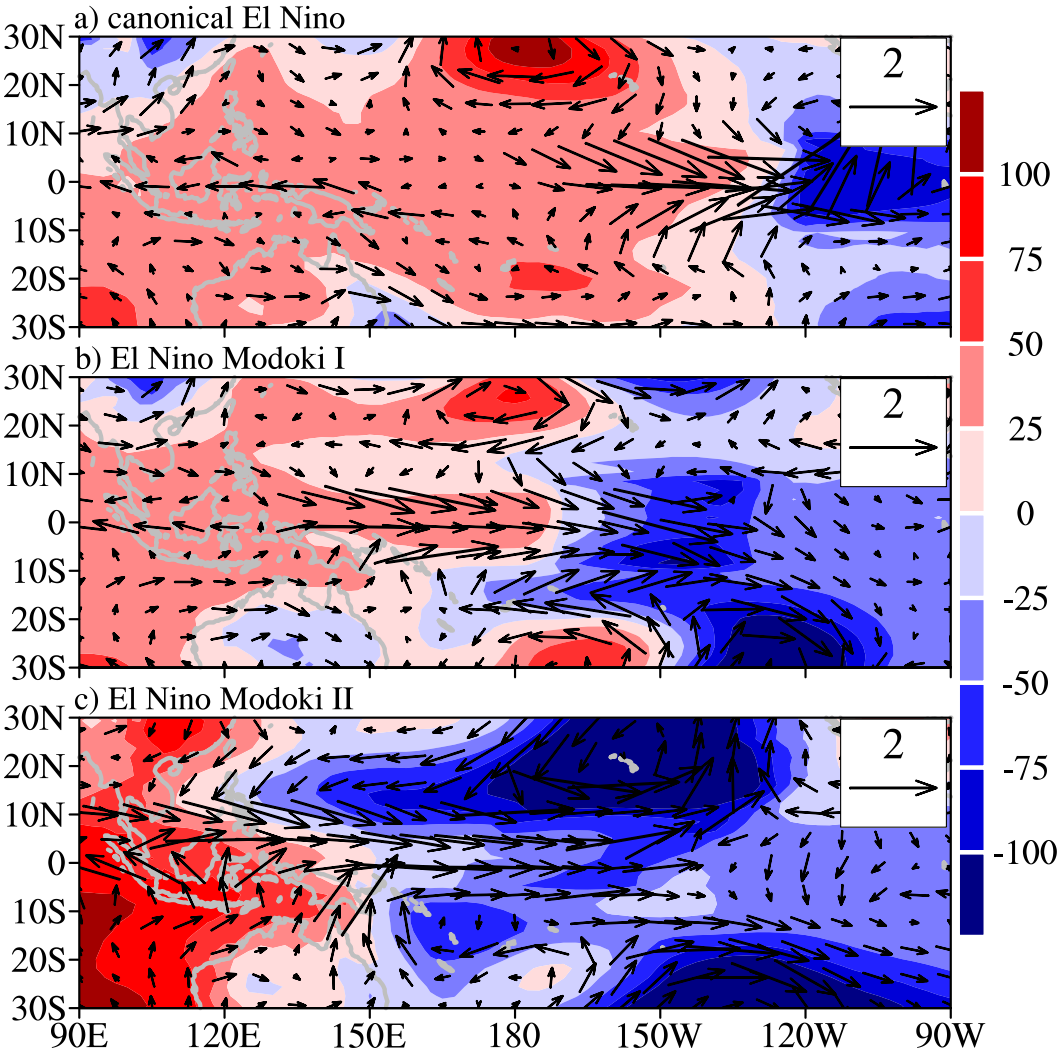

FIG. 13. The differences of the SLP (shading; Pa) and 850-hPa wind anomalies (vector; $m\,s^{-1}$) averaged in boreal autumn (October and November) between sensitivity and control experiments for (a) canonical El Niño, (b) El Niño Modoki I, and (c) El Niño Modoki II.

observed results by Wang and Wang (2013). For canonical El Niño (Fig. 13a), in response to the warm SST anomalies in the equatorial eastern Pacific, a pair of anomalous cyclones is located on both sides of the equator (Gill 1980), associated with significant equatorial westerly anomalies. As a Rossby wave response, an anomalous anticyclone occurs near the Philippine Sea (Wang et al. 2000; Wang 2002), inducing southwesterly anomalies over the SCS. Similar to canonical El Niño, the anomalous anticyclone exists over the Philippine Sea for El Niño Modoki I, with a weaker intensity (Fig. 13b). The locations of the westerly wind anomalies and two cyclones straddled on the equator are farther westward. However, for El Niño Modoki II, the anticyclone shifts westward to Southeast Asia and an anomalous cyclone appears near the Philippine Sea, inducing northeasterly anomalies over the SCS (Fig. 13c). These numerical experiments further confirm the atmospheric response to different types of El Niño events as we discussed above.

7. Summary and discussion

The interannual variation of the SCS SST is closely related to El Niño events (Tomita and Yasunari 1996; Ose et al. 1997; Qu et al. 2004; Wang et al. 2006) and exhibits different features for canonical El Niño and El Niño Modoki events (Liu et al. 2014). Recently, El Niño Modoki events can be further separated into two types, El Niño Modoki I and II, with significantly different impacts on rainfall in southern China, tropical cyclone activity in the western Pacific, and the IOD (Wang and Wang 2013; Wang and Wang 2014; Wang et al. 2014). In this paper,

TABLE 1. Years of the IOD and pure IOD events during 1958–2008.

Positive IOD	Pure positive IOD	Negative IOD	Pure negative IOD
1961	1961	1958	1959
1963	1994	1959	1960
1972	2006	1960	1980
1982	2007	1964	1996
1987	—	1980	—
1991	—	1992	—
1994	—	1996	—
1997	—	—	—
2006	—	—	—
2007	—	—	—

different responses of SCS SST anomalies to three types of El Niño events (canonical El Niño, El Niño Modoki I, and El Niño Modoki II) during developing autumn are explored, and the associated mechanisms are also studied.

The warm SST anomalies appear in the SCS for canonical El Niño and El Niño Modoki I, while the SCS shows a cold state for El Niño Modoki II during developing autumn. Based on the ocean heat budget analysis, the SST variations in autumn associated with three types of El Niño events are attributed to the net surface heat flux. Compared with the net heat flux, the contributions of oceanic processes (i.e., Ekman advection, geostrophic advection, and entrainment heat flux) to the SCS SST tendency in developing autumn of various types of El Niño events are small. An anomalous anticyclone resides near the Philippine Sea for canonical El Niño and El Niño Modoki I. The anticyclone induces the southerly anomalies over the SCS that weaken the climatological northeasterly wind. The diminished wind speed reduces heat loss from the ocean via the latent heat flux, and thus the SCS tends to be warm. However, for El Niño Modoki II, the anomalous anticyclone shifts westward, and the SCS is associated with the northeasterly anomalies. Thus, the strengthened northeasterly enhances the loss of latent heat from the ocean to cool the SCS for El Niño Modoki II.

The ENSO-induced large-scale circulations influence not only the changes of the latent heat flux, but also the shortwave radiation flux in the SCS. The anomalous anticyclone circulations over the Philippine Sea and SCS for various types of El Niño events (Fig. 10) could suppress the convection over the SCS, and thus reduce the cloud cover (Fig. 11), increasing shortwave radiation (Figs. 8d–f) to warm the SCS. This means that the latent heat flux combined with the shortwave radiation contributes to the SCS warming for canonical El Niño [consistent with Wang et al. (2006); Chen et al. 2007] and El Niño Modoki I. However, since the cooling effect of the latent heat flux is larger than the warming effect of the shortwave radiation flux for El Niño Modoki II, the SCS SST tends to be cool.

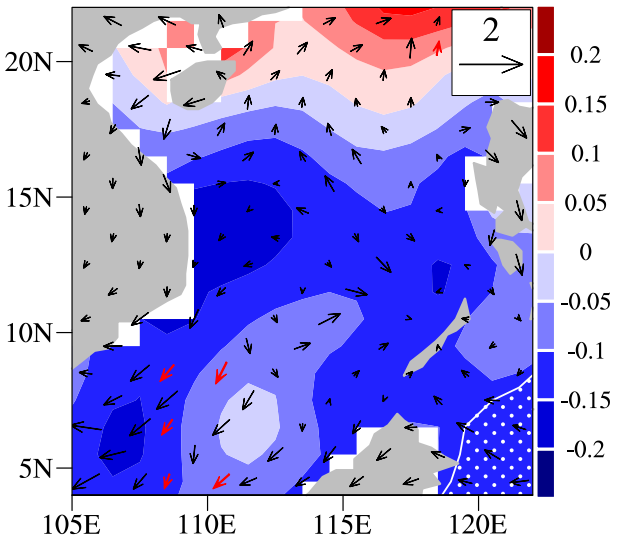

FIG. 14. Composite difference of the SCS SST anomalies (shading; °C) and 10-m wind anomalies (vector; m s^{-1}) between the pure positive and negative IOD events during boreal autumn (ON). The white contours and the area filled with white dots (red vectors) indicate the composite SST (meridional wind) anomalies exceeding the 90% significant level, based on a Student's *t* test. The HadISST dataset and ICOADS were used.

Since El Niño Modoki occurs more frequently under the projected global warming scenarios from simulations from phases 3 and 5 of the Coupled Model Intercomparison Project (CMIP3 and CMIP5) (Yeh et al. 2009; Kim and Yu 2012), it is necessary to explore the impacts of El Niño Modoki on global climate. Our results provide an impact for the SCS responses to El Niño Modoki, which is helpful to improve the understanding of the regional climate under global warming.

Besides the impacts of the tropical Pacific, climate variability in the SCS and the western tropical Pacific is also influenced by the Indian Ocean (Saji et al. 1999; Webster et al. 1999; Saji and Yamagata 2003; Yamagata et al. 2004; Annamalai et al. 2005; Xie et al. 2009). Since the IOD is a distinct mode in the Indian Ocean during boreal autumn (Saji et al. 1999) and is clearly associated with various types of El Niño events (Wang and Wang 2014), we also examine the responses of the SCS SST anomalies to the IOD. The Indian Ocean dipole mode index (DMI) is calculated as the SST anomaly difference between the western (10°S–10°N, 50°–70°E) and southeastern (10°S–0°, 90°–110°E) tropical Indian Ocean (Saji et al. 1999). Following the definition by Rao et al. (2002), positive (negative) IOD events are identified as the years in which the normalized annual mean of DMI is larger (lower) than 1.0

(−1.0). According to the criteria, 10 (7) positive (negative) IOD events are selected during 1958–2008 (Table 1), which is consistent with the results in Rao et al. (2002) but with a shorter time period. The positive IOD co-occurs with canonical El Niño and El Niño Modoki I, while some negative IOD events accompany with El Niño Modoki II and La Niña (Ashok et al. 2003; Meyers et al. 2007; Wang and Wang 2014). To separate the influences of ENSO, the "pure positive IOD" events are defined without co-occurrence of canonical El Niño and El Niño Modoki I, and the "pure negative IOD" events are identified with the absence of El Niño Modoki II and La Niña (Table 1). Compared with the SCS SST variations associated with various types of El Niño events (Fig. 3), the composite differences of the SST anomalies between pure positive IOD and negative IOD are weaker with positive (negative) values in the northern (southern) SCS during boreal autumn, and they are not significant together with the 10-m wind anomalies (Fig. 14).

Moreover, the atmospheric responses to IOD forcing are also simulated by CAM4, via two sensitivity experiments. The experiments are forced with the sum of climatological SST and composited SST anomalies in the tropical Indian Ocean (10°S–10°N, 30°–110°E) during pure positive IOD and negative IOD events (Table 1), respectively. The composite difference of 10-m wind anomalies between these two experiments is nearly imperceptible (not shown), which is in accordance with the observed results (Fig. 14). The model results further corroborate that the SCS SST variations are less influenced by the IOD. In other words, various types of El Niño events are responsible for the changes of the SCS SST.

Acknowledgments. This work was supported by the Strategic Priority Research Program of the Chinese Academy of Sciences (Grant XDA11010403), the CAS/SAFEA International Partnership Program for Creative Research Teams, National Natural Science Foundation of China (Grants 41422601, 41376025 and 41376024), the National Basic Research Program of China (2013CB430301 and 2013CB430302), the Project of Global Change and Air–Sea Interaction under Contract GASI-03-IPOVAI-04, the National Oceanic and Atmospheric Administration (NOAA) Climate Program Office, and the base funding of NOAA/Atlantic Oceanographic and Meteorological Laboratory (AOML).

REFERENCES

Alexander, M. A., I. Bladé, M. Newman, J. R. Lanzante, N.-C. Lau, and J. D. Scott, 2002: The atmospheric bridge: The influence of ENSO teleconnections on air–sea interaction over the global oceans. *J. Climate*, **15**, 2205–2231, doi:10.1175/1520-0442(2002)015<2205:TABTIO>2.0.CO;2.

Annamalai, H., P. Liu, and S. Xie, 2005: Southwest Indian Ocean SST variability: Its local effect and remote influence on Asian monsoons. *J. Climate*, **18**, 4150–4167, doi:10.1175/JCLI3533.1.

Ashok, K., Z. Guan, and T. Yamagata, 2003: A look at the relationship between the ENSO and the Indian Ocean dipole. *J. Meteor. Soc. Japan*, **81**, 41–56, doi:10.2151/jmsj.81.41.

——, S. K. Behera, S. A. Rao, H. Weng, and T. Yamagata, 2007: El Niño Modoki and its possible teleconnection. *J. Geophys. Res.*, **112**, C11007, doi:10.1029/2006JC003798.

Carton, J. A., and B. S. Giese, 2008: A reanalysis of ocean climate using Simple Ocean Data Assimilation (SODA). *Mon. Wea. Rev.*, **136**, 2999–3017, doi:10.1175/2007MWR1978.1.

Chen, J., T. Li, and C. Shih, 2007: Fall persistence barrier of sea surface temperature in the South China Sea associated with ENSO. *J. Climate*, **20**, 158–172, doi:10.1175/JCLI4000.1.

Chen, W., H. Graf, and R. Huang, 2000: The interannual variability of East Asian winter monsoon and its relation to the summer monsoon. *Adv. Atmos. Sci.*, **17**, 48–60, doi:10.1007/s00376-000-0042-5.

Chou, S.-H., W. Zhao, and M.-D. Chou, 2000: Surface heat budgets and sea surface temperature in the Pacific warm pool during TOGA COARE. *J. Climate*, **13**, 634–649, doi:10.1175/1520-0442(2000)013<0634:SHBASS>2.0.CO;2.

Chu, P. C., and C. P. Chang, 1997: South China Sea warm pool in boreal spring. *Adv. Atmos. Sci.*, **14**, 195–206, doi:10.1007/s00376-997-0019-8.

——, N. L. Edmons, and C. Fan, 1999: Dynamical mechanisms for the South China Sea seasonal circulation and thermohaline variabilities. *J. Phys. Oceanogr.*, **29**, 2971–2989, doi:10.1175/1520-0485(1999)029<2971:DMFTSC>2.0.CO;2.

Ding, Y., C. Li, and Y. Liu, 2004: Overview of the South China Sea Monsoon Experiment. *Adv. Atmos. Sci.*, **21**, 343–360, doi:10.1007/BF02915563.

Ebita, A., and Coauthors, 2011: The Japanese 55-Year Reanalysis "JRA-55": An interim report. *SOLA*, **7**, 149–152, doi:10.2151/sola.2011-038.

Fang, G., H. Chen, Z. Wei, Y. Wang, X. Wang, and C. Li, 2006: Trends and interannual variability of the South China Sea surface winds, surface height, and surface temperature in the recent decade. *J. Geophys. Res.*, **111**, C11S16, doi:10.1029/2005JC003276.

Gent, P., and Coauthors, 2011: The Community Climate System Model version 4. *J. Climate*, **24**, 4973–4991, doi:10.1175/2011JCLI4083.1.

Gill, A., 1980: Some simple solutions for heat-induced tropical circulation. *Quart. J. Roy. Meteor. Soc.*, **106**, 447–462, doi:10.1002/qj.49710644905.

Gong, D., Y. Pan, and J. Wang, 2004: Changes in extreme daily mean temperatures in summer in eastern China during 1955–2000. *Theor. Appl. Climatol.*, **77**, 25–37, doi:10.1007/s00704-003-0019-2.

Gupta, S. K., N. A. Ritchey, A. C. Wilber, C. H. Whitlock, G. G. Gibson, and P. W. Stackhouse Jr., 1999: A climatology of surface radiation budget derived from satellite data. *J. Climate*, **12**, 2691–2710, doi:10.1175/1520-0442(1999)012<2691:ACOSRB>2.0.CO;2.

Hong, C.-C., Y.-H. Li, T. Li, and M.-Y. Lee, 2011: Impacts of central Pacific and eastern Pacific El Niños on tropical cyclone tracks over the western North Pacific. *Geophys. Res. Lett.*, **38**, L16712, doi:10.1029/2011GL048821.

Kajikawa, Y., and B. Wang, 2012: Interdecadal change of the South China Sea summer monsoon onset. *J. Climate*, **25**, 3207–3218, doi:10.1175/JCLI-D-11-00207.1.

Kalnay, E., and Coauthors, 1996: The NCEP/NCAR 40-Year Reanalysis Project. *Bull. Amer. Meteor. Soc.*, **77**, 437–471, doi:10.1175/1520-0477(1996)077<0437:TNYRP>2.0.CO;2.

Kao, H.-Y., and J.-Y. Yu, 2009: Contrasting eastern-Pacific and central-Pacific types of ENSO. *J. Climate*, **22**, 615–632, doi:10.1175/2008JCLI2309.1.

Kim, J.-S., W. Zhou, X. Wang, and S. Jain, 2012: El Niño Modoki and the summer precipitation variability over South Korea: A diagnostic study. *J. Meteor. Soc. Japan*, **90**, 673–684, doi:10.2151/jmsj.2012-507.

Kim, S. T., and J.-Y. Yu, 2012: The two types of ENSO in CMIP5 models. *Geophys. Res. Lett.*, **39**, L11704, doi:10.1029/2012GL052006.

Klein, S. A., B. J. Soden, and N.-C. Lau, 1999: Remote sea surface temperature variations during ENSO: Evidence for a tropical atmospheric bridge. *J. Climate*, **12**, 917–932, doi:10.1175/1520-0442(1999)012<0917:RSSTVD>2.0.CO;2.

Kug, J.-S., F.-F. Jin, and S.-I. An, 2009: Two types of El Niño events: Cold tongue El Niño and warm pool El Niño. *J. Climate*, **22**, 1499–1515, doi:10.1175/2008JCLI2624.1.

Larkin, N. K., and D. E. Harrison, 2005: Global seasonal temperature and precipitation anomalies during El Niño autumn and winter. *Geophys. Res. Lett.*, **32**, L16705, doi:10.1029/2005GL022860.

Lee, T., and M. J. McPhaden, 2010: Increasing intensity of El Niño in the central-equatorial Pacific. *Geophys. Res. Lett.*, **37**, L14603, doi:10.1029/2010GL044007.

Liang, J., Z. Wen, J. Chen, and L. Wu, 2013: Characteristics of tropical sea surface temperature anomalies and their influences on the onset of South China Sea summer monsoon. *Atmos. Oceanic Sci. Lett.*, **6**, 266–272, doi:10.3878/j.issn.1674-2834.13.0026.

Ling, Z., G. Wang, C. Wang, and Z.-S. Fan, 2011: Different effects of tropical cyclones generated in the South China Sea and the northwest Pacific on the summer South China Sea circulation. *J. Oceanogr.*, **67**, 347–355, doi:10.1007/s10872-011-0044-1.

Liu, Q., D. Wang, Y. Jia, and Y. Du, 2002: Seasonal variation and formation mechanism of the South China Sea warm water. *Acta Oceanol. Sin.*, **21**, 331–343.

——, X. Jiang, S. Xie, and W. T. Liu, 2004: A gap in the Indo-Pacific warm pool over the South China Sea in boreal winter: Seasonal development and interannual variability. *J. Geophys. Res.*, **109**, C07012, doi:10.1029/2003JC002179.

Liu, Q.-Y., M. Feng, and D. Wang, 2011: ENSO-induced interannual variability in the southeastern South China Sea. *J. Oceanogr.*, **67**, 127–133, doi:10.1007/s10872-011-0002-y.

——, D. Wang, X. Wang, Y. Shu, Q. Xie, and J. Chen, 2014: Thermal variations in the South China Sea associated with the eastern and central Pacific El Niño events and their mechanisms. *J. Geophys. Res. Oceans*, **119**, 8955–8972, doi:10.1002/2014JC010429.

Meyers, G., P. McIntosh, L. Pigot, and M. Pook, 2007: The years of El Niño, La Niña, and interactions with the tropical Indian Ocean. *J. Climate*, **20**, 2872–2880, doi:10.1175/JCLI4152.1.

Monterey, G., and S. Levitus, 1997: *Seasonal Variability of Mixed Layer Depth for the World Ocean*. NOAA Atlas NESDIS 14, 96 pp. and 87 figs.

Neale, R., J. Richter, S. Park, P. H. Lauritzen, S. J. Vavrus, P. J. Rasch, and M. Zhang, 2013: The mean climate of the Community Atmosphere Model (CAM4) in forced SST and fully coupled experiments. *J. Climate*, **26**, 5150–5168, doi:10.1175/JCLI-D-12-00236.1.

Ning, L., and Y. Qian, 2009: Interdecadal change in extreme precipitation over South China and its mechanism. *Adv. Atmos. Sci.*, **26**, 109–118, doi:10.1007/s00376-009-0109-x.

Ose, T., Y. Song, and A. Kitoh, 1997: Sea surface temperature in the South China Sea: An index for the Asian monsoon and ENSO system. *J. Meteor. Soc. Japan*, **75**, 1091–1107.

Qiu, B., 2000: Interannual variability of the Kuroshio Extension System and its impact on the wintertime SST field. *J. Phys. Oceanogr.*, **30**, 1486–1502, doi:10.1175/1520-0485(2000)030<1486:IVOTKE>2.0.CO;2.

Qu, T., 2000: Upper-layer circulation in the South China Sea. *J. Phys. Oceanogr.*, **30**, 1450–1460, doi:10.1175/1520-0485(2000)030<1450:ULCITS>2.0.CO;2.

——, 2001: Role of ocean dynamics in determining the mean seasonal cycle of the South China Sea surface temperature. *J. Geophys. Res.*, **106**, 6943–6955, doi:10.1029/2000JC000479.

——, H. Mitsudera, and T. Yamagata, 2000: The intrusion of the North Pacific waters into the South China Sea. *J. Geophys. Res.*, **105**, 6415–6424, doi:10.1029/1999JC900323.

——, Y. Y. Kim, M. Yaremchuk, T. Tozuka, A. Ishida, and T. Yamagata, 2004: Can Luzon Strait transport play a role in conveying the impact of ENSO to the South China Sea? *J. Climate*, **17**, 3644–3657, doi:10.1175/1520-0442(2004)017<3644:CLSTPA>2.0.CO;2.

Rao, S. A., S. K. Behera, Y. Masumoto, and T. Yamagata, 2002: Interannual subsurface variability in the tropical Indian Ocean with a special emphasis on the Indian Ocean dipole. *Deep-Sea Res. II*, **49**, 1549–1572, doi:10.1016/S0967-0645(01)00158-8.

Rasmusson, E. M., and T. H. Carpenter, 1982: Variation in tropical sea surface temperature and surface wind fields associated with Southern Oscillation/El Niño. *Mon. Wea. Rev.*, **110**, 354–384, doi:10.1175/1520-0493(1982)110<0354:VITSST>2.0.CO;2.

Rayner, N. A., D. E. Parker, E. B. Horton, C. K. Folland, L. V. Alexander, D. P. Rowell, E. C. Kent, and A. Kaplan, 2003: Global analysis of sea surface temperature, sea ice and night marine air temperature since the late nineteenth century. *J. Geophys. Res.*, **108**, 4407, doi:10.1029/2002JD002670.

Saji, N. H., and T. Yamagata, 2003: Possible impacts of Indian Ocean dipole mode events on global climate. *Climate Res.*, **25**, 151–169, doi:10.3354/cr025151.

——, B. N. Goswami, P. N. Vinayachandran, and T. Yamagata, 1999: A dipole mode in the tropical Indian Ocean. *Nature*, **401**, 360–363.

Shaw, P. T., and S. Y. Chao, 1994: Surface circulation in the South China Sea. *Deep-Sea Res. I*, **41**, 1663–1683.

——, ——, and L. L. Fu, 1999: Sea surface height variations in the South China Sea from satellite altimetry. *Oceanol. Acta*, **22**, 1–17, doi:10.1016/S0399-1784(99)80028-0.

Tian, J., Q. Yang, X. Liang, L. Xie, D. Hu, F. Wang, and T. Qu, 2006: Observation of Luzon Strait transport. *Geophys. Res. Lett.*, **33**, L19607, doi:10.1029/2006GL026272.

Tomita, T., and T. Yasunari, 1996: Role of the northeast winter monsoon on the biennial oscillation of the ENSO/monsoon system. *J. Meteor. Soc. Japan*, **74**, 399–413.

Trenberth, K. E., G. W. Branstator, D. Karoly, A. Kumar, N.-C. Lau, and C. Ropelewski, 1998: Progress during TOGA in understanding and modeling global teleconnections associated with tropical sea surface temperature. *J. Geophys. Res.*, **103**, 14 291–14 324, doi:10.1029/97JC01444.

Wang, B., R. Wu, and X. Fu, 2000: Pacific–East Asian teleconnection: How does ENSO affect East Asian climate? *J. Climate*, **13**, 1517–1536, doi:10.1175/1520-0442(2000)013<1517:PEATHD>2.0.CO;2.

Wang, C., 2002: Atmospheric circulation cells associated with the El Niño–Southern Oscillation. *J. Climate*, **15**, 399–419, doi:10.1175/1520-0442(2002)015<0399:ACCAWT>2.0.CO;2.

——, and X. Wang, 2013: Classifying El Niño Modoki I and II by different impacts on rainfall in southern China and typhoon tracks. *J. Climate*, **26**, 1322–1338, doi:10.1175/JCLI-D-12-00107.1.

——, R. H. Weisberg, and J. I. Virmani, 1999: Western Pacific interannual variability associated with the El Niño–Southern Oscillation. *J. Geophys. Res.*, **104** (C3), 5131–5149, doi:10.1029/1998JC900090.

——, W. Wang, D. Wang, and Q. Wang, 2006: Interannual variability of the South China Sea associated with El Niño. *J. Geophys. Res.*, **111**, C03023, doi:10.1029/2005JC003333 .

Wang, D., Q. Xie, Y. Du, W. Wang, and J. Chen, 2002: The 1997–1998 warm event in the South China Sea. *Chin. Sci. Bull.*, **47**, 1221–1227, 10.1007/BF02907614.

Wang, G., Z. Ling, and C. Wang, 2009: Influence of tropical cyclones on seasonal ocean circulation in the South China Sea. *J. Geophys. Res.*, **114**, C10022, doi:10.1029/2009JC005302.

Wang, W., and C. Wang, 2006: Formation and decay of the spring warm pool in the South China Sea. *Geophys. Res. Lett.*, **33**, L02615, doi:10.1029/2005GL025097.

Wang, X., and C. Wang, 2014: Different impacts of various El Niño events on the Indian Ocean dipole. *Climate Dyn.*, **42**, 991–1005, doi:10.1007/s00382-013-1711-2.

——, D. Wang, W. Zhou, and C. Li, 2012: Interdecadal modulation of the influence of La Niña events on mei-yu rainfall over the Yangtze River Valley. *Adv. Atmos. Sci.*, **29**, 157–168, doi:10.1007/s00376-011-1021-8.

——, W. Zhou, C. Li, and D. Wang, 2014: Comparison of the impact of two types of El Niño on tropical cyclone genesis over the South China Sea. *Int. J. Climatol.*, **34**, 2651–2660, doi:10.1002/joc.3865.

Webster, P. J., A. M. Moore, J. P. Loschnigg, and R. R. Leben, 1999: Coupled ocean–atmosphere dynamics in the Indian Ocean during 1997–98. *Nature*, **401**, 356–360, doi:10.1038/43848.

Weisberg, R. H., and C. Wang, 1997: A western Pacific oscillator paradigm for the El Niño–Southern Oscillation. *Geophys. Res. Lett.*, **24**, 779–782, doi:10.1029/97GL00689.

Weng, H., K. Ashok, S. K. Behera, S. A. Rao, and T. Yamagata, 2007: Impacts of recent El Niño Modoki on dry/wet conditions in the Pacific Rim during boreal summer. *Climate Dyn.*, **29**, 113–129, doi:10.1007/s00382-007-0234-0.

Woodruff, S. D., and Coauthors, 2011: ICOADS release 2.5: Extensions and enhancements to the surface marine meteorological archive. *Int. J. Climatol.*, **31**, 951–967, doi:10.1002/joc.2103.

Wu, R., Z. Wen, S. Yang, and Y. Li, 2010: An interdecadal change in southern China summer rainfall around 1992/93. *J. Climate*, **23**, 2389–2403, doi:10.1175/2009JCLI3336.1.

——, W. Chen, G. Wang, and K. Hu, 2014: Relative contribution of ENSO and East Asian winter monsoon to the South China Sea SST anomalies during ENSO decaying years. *J. Geophys. Res.*, **119**, 5046–5064, doi:10.1002/2013JD021095.

Wyrtki, K., 1961: Physical oceanography of the Southeast Asian waters: Scientific results of marine investigations of the South China Sea and the Gulf of Thailand. NAGA Rep. 2, Scripps Institution of Oceanography, 195 pp.

Xiang, B., and B. Wang, 2013: Mechanisms for the advanced Asian summer monsoon onset since the mid-to-late 1990s. *J. Climate*, **26**, 1993–2009, doi:10.1175/JCLI-D-12-00445.1.

Xie, S.-P., Q. Xie, D. Wang, and W. T. Liu, 2003: Summer upwelling in the South China Sea and its role in regional climate variations. *J. Geophys. Res.*, **108**, 3261, doi:10.1029/2003JC001867.

——, K. Hu, J. Hafner, H. Tokinaga, Y. Du, G. Huang, and T. Sampe, 2009: Indian Ocean capacitor effect on Indo-western Pacific climate during the summer following El Niño. *J. Climate*, **22**, 730–747, doi:10.1175/2008JCLI2544.1.

Yamagata, T., S. K. Behara, J. Luo, S. Masson, M. Jury, and S. A. Rao, 2004: Coupled ocean–atmosphere variability in the tropical Indian Ocean. *Earth's Climate*, Geophys. Monogr., Vol. 147, Amer. Geophys. Union, 189–211, doi:10.1029/147GM12.

Yang, H., Q. Liu, Z. Liu, D. Wang, and X. Liu, 2002: A general circulation model study of the dynamics of the upper ocean circulation of the South China Sea. *J. Geophys. Res.*, **107**, 3085, doi:10.1029/2001JC001084.

Yeh, S.-W., J.-S. Kug, B. Dewitte, M.-H. Kwon, B. P. Kirtman, and F.-F. Jin, 2009: El Niño in a changing climate. *Nature*, **461**, 511–514, doi:10.1038/nature08316.

Yu, J.-Y., and H.-Y. Kao, 2007: Decadal changes of ENSO persistence barrier in SST and ocean heat content indices: 1958–2001. *J. Geophys. Res.*, **112**, D13106, doi:10.1029/2006JD007654.

Zhang, Y., D. Wang, H. Xia, and L. Zeng, 2012: The seasonal variability of an air–sea heat flux in the northern South China Sea. *Acta Oceanol. Sin.*, **31**, 79–86, doi:10.1007/s13131-012-0238-4.

Zhou, L., C. Tam, W. Zhou, and J. C. L. Chan, 2010: Influence of South China Sea SST and the ENSO on winter rainfall over South China. *Adv. Atmos. Sci.*, **27**, 832–844, doi:10.1007/s00376-009-9102-7.